



Numerical and Experimental Investigation into the Jet and Dispersion of CO₂ from Pressurized Transportation Pipelines

C. Xu[†], X. Zhang, Z. Ding and S. Wang

*Key Laboratory of Energy Thermal Conversion and Control of Ministry of Education, Southeast University,
Nanjing 210096, P. R. China*

Corresponding Author Email: chuanlongxu@seu.edu.cn

(Received October 20, 2015; accepted December 10, 2015)

ABSTRACT

In carbon capture and storage system, the captured CO₂ from energy production processes is compressed to high pressures, transported to a storage site, and then injected into a suitable geologic formation. The leakages from high pressure transportation pipelines would pose hazard to the environment and people. In this paper, a laboratory scale rig for simulating CO₂ pipeline leakage is built, and a two-dimensional model is further developed to study the complex behavior of the jet and dispersion of CO₂ from the rig at continuous leakage flowrate. In view of the phase-change heat transfer of CO₂, a multiphase flow model is used to simulate the jet and dispersion of CO₂ gas-liquid two-phase flow. The Euler/Lagrange model and particle stochastic trajectory model are applied to describing the development process of the jet and dispersion of CO₂. The computational fluid dynamics software Fluent is employed to calculate the flow field. To prove the validity of the numerical models, an infrared thermography is used to record the temperature field near the leakage orifice during experiments.

Keywords: Computational Fluid Dynamics (CFD); Carbon Capture and Storage; CO₂; Leakage; Jet; Transportation pipeline.

NOMENCLATURE

P	static pressure of CO ₂	d_p	droplet size
ρ	CO ₂ gas density	τ	relaxation time of droplet
μ	dynamic viscosity of CO ₂ gas	m_p	mass of droplet
c	specific heat capacity of CO ₂	A_p	surface area of droplet
c_k	thermal conductivity of CO ₂ flow	M	molecular weight of CO ₂
T	temperature of CO ₂	T_p	surface temperature of droplet
k	turbulent energy	R	gas constant
ε	turbulent dissipation rate	h	convective heat transfer coefficient

1. INTRODUCTION

The rising CO₂ concentration has led to increasing ocean acidification and may be contributing to climate change and a rising of global temperatures. Carbon Capture and Storage (CCS) could potentially capture around 90% of the CO₂ emitted when fossil fuels such as coal are used, and thus has the potential to mitigate climate change by reducing CO₂ emissions. In CCS process CO₂ is captured from energy production processes, compressed to high pressures, transported to a storage site, and then injected into a suitable

geologic formation. Transporting CO₂ from point-of-capture to storage sites is an important linking step in the CCS chain. According to the research of Eldevik *et al.* (2009) and Svensson *et al.* (2004), although CO₂ is transported via pipelines, ships, and tanker trucks, pipeline transport is considered to be the most cost-effective and reliable method for transporting CO₂ to on-shore and off-shore underground storage sites for CCS. However, the study of Molag and Dam (2011) illustrated that if a high pressure pipeline among extensive networks of CO₂ transportation facilities suffers a major fracture due to third-party intrusion accident or component failure, the compressed CO₂

would rapidly expand and cool. In the case of pure CO₂, this would initially form a vapor cloud around the fracture, followed by the formation of solid CO₂ ‘snow’. During surface transportation, the leakages from high pressure pipelines would result in damage to the environment and hazard to people in populated areas, for carbon dioxide is an asphyxiant and toxic at high concentrations. Shape and size of the formed cloud and the velocity of CO₂ in dispersing to safe concentration will be dependent on atmospheric conditions (stability, wind speed and direction, turbulence, pressure and temperature) and site topography. Therefore, it is critical to investigate the complex behavior of the jet and dispersion of CO₂ from pressurized transportation pipelines for the future development of CCS and the formulation of safety and risk assessment tools.

The methods for investigating the jet and dispersion of CO₂ from pressurized transportation pipelines mainly include field test, wind tunnel test and numerical simulation. However, due to huge cost, long experimental cycle and the difficulty in simulating industrial-scale CO₂ pipeline leakage conditions for the field test and wind tunnel test methods, numerical simulation and small-scale experimental test are considered useful tools to investigate the jet and dispersion of CO₂. Up to date, many simulation works (Molag *et al.* 2011, Mazzoldi *et al.* 2008a,b, 2009, 2011; Cortis, 2009; Witlox *et al.* 2009; Vagesh and GexCon, 2013a,b) on the jet and dispersion of CO₂ during pipelines transport have been performed. In combination with the Euler model of fluid dynamics based on N-S equation, Mazzoldi A. *et al.* (2008a,b, 2009, 2011) employed Fluidyn-PANACHE software to study the effects of the initial speed of the leaking flow of supercritical CO₂ on downwind CO₂ concentration contours under different environmental conditions, and also to develop a model for evaluating the sublimation rate of a frozen CO₂ bank created after the leakage of the CO₂ gas from a high pressure CCS transportation facility with the aim of considering possible acute health effects on people. These simulation results were compared with those from Gaussian models for steady state dispersion of CO₂. Cortis *et al.* (2009) modeled dense gas dispersion using the steady-state Reynolds averaged Navier-Stokes equations with density-dependence in the gravity term, and further studied the effects of density on the transport behavior of CO₂ plumes seeping out of the ground in a two-dimensional mesoscale space. Witlox *et al.* (2009) numerically investigated the discharge and subsequent atmospheric dispersion for carbon dioxide releases allowing for the occurrence of the fluid to solid transition in the consequence modelling package Phast. The results illustrated that the failure to account for solid effects in the discharge modelling results in a too low post-expansion temperature and in a too high post-expansion liquid fraction. Vagesh *et al.* (2013a, b) established an Eulerian-Lagrangian combined with three-phase model, and the FLACS and CFX were further employed to calculate the dispersion of CO₂ gas cloud in the three-dimensional space. The geographic

information system (GIS) was also used to study the effects of complex topography and atmospheric conditions on CO₂ dispersion. These developed models provided the insights into the jet and dispersion of CO₂ from pressurized transportation pipelines. However, in these models, the behavior of jet and dispersion of CO₂ from pressurized transportation pipeline was modeled as a single phase to reduce the computational time. In fact, the jet flow is a typical multiphase flow process, involving air, CO₂ gas, CO₂ droplets, and even solid dry ice.

The present work in this paper aims to develop a two-dimensional model to study the jet and dispersion of CO₂ from the CCS transportation pipelines at continuous leakage flowrate. Euler method is used to solve the mixture of CO₂ gas and entrained air, and the evaporation and dispersion of CO₂ droplet is solved by Lagrange method. During leakage, CO₂ droplets interact with the surrounding air vortex, which causes the motion of CO₂ droplets affected by random forces. The particle stochastic trajectory model is applied to solving the turbulence of CO₂ droplets. Further a laboratory scale rig for simulating the leakage of CO₂ from a transportation pipeline is built to validate the model. Finally, a series of simulations and experiments are carried out, and results are presented and analysed.

2. COMPUTATIONAL MODELS

2.1. Gas Phase

Mathematical models of the jet and dispersion of CO₂ are established based on the conservation equations of mass, momentum, and energy after leakage. The local averaged equations of continuity and motion are used to compute the motion of the gas phase, given respectively by

$$\frac{\partial \rho}{\partial t} + \nabla \cdot (\rho u) = 0 \quad (1)$$

$$\begin{aligned} & \frac{\partial(\rho u)}{\partial t} + \frac{\partial}{\partial x_i}(\rho u_i u_i) + \frac{\partial}{\partial x_j}(\rho u_i u_j) \\ & = \frac{\partial}{\partial x_i}(\mu \frac{\partial u_i}{\partial x_i}) + \frac{\partial}{\partial x_j}(\mu \frac{\partial u_j}{\partial x_j}) - \frac{\partial P}{\partial x_i} + S_i \end{aligned} \quad (2)$$

$$\begin{aligned} & \frac{\partial(\rho u_j)}{\partial t} + \frac{\partial}{\partial x_i}(\rho u_j u_i) + \frac{\partial}{\partial y}(\rho u_j u_j) \\ & = \frac{\partial}{\partial x_i}(\mu \frac{\partial u_j}{\partial x_i}) + \frac{\partial}{\partial x_j}(\mu \frac{\partial u_j}{\partial x_j}) - \frac{\partial P}{\partial x_i} + S_j \end{aligned} \quad (3)$$

where u are the gas velocity vector (u_i, u_j), x is the coordinate (x_i, x_j), and S_i and S_j are source terms, respectively.

The energy equation is

$$\begin{aligned} & \frac{\partial(\rho T)}{\partial t} + \frac{\partial}{\partial x_i}(\rho u_i T) + \frac{\partial}{\partial x_j}(\rho u_j T) \\ &= \frac{\partial}{\partial x_i} \left(\frac{c_k}{c} \frac{\partial T}{\partial x_i} \right) + \frac{\partial}{\partial x_j} \left(\frac{c_k}{c} \frac{\partial T}{\partial x_j} \right) + S_T \end{aligned} \quad (4)$$

where S_T is the internal heat source.

The gas component equation is

$$\begin{aligned} & \frac{\partial(\rho c_s)}{\partial t} + \frac{\partial}{\partial x_i}(\rho u_i c_s) + \frac{\partial}{\partial x_j}(\rho u_j c_s) \\ &= \frac{\partial}{\partial x_i} \left(D_s \frac{\partial(\rho c_s)}{\partial x_i} \right) + \frac{\partial}{\partial x_j} \left(D_s \frac{\partial(\rho c_s)}{\partial x_j} \right) + S_s \end{aligned} \quad (5)$$

where c_s is the mass fraction of the gas (s), D_s is the diffusion coefficient of the gas (s), S_s is the chemical reaction rate of the gas (s).

The realizable $k-\varepsilon$ model is employed in this paper. The governing transport equations for the turbulent energy k and the turbulent dissipation rate ε are

$$\frac{\partial(\rho k)}{\partial t} + \nabla \cdot (\rho k u) = \nabla \cdot \left(\left(\mu + \frac{\mu_t}{\sigma_k} \right) \nabla \cdot k \right) + G_k - \rho \varepsilon \quad (6)$$

$$\frac{\partial(\rho \varepsilon)}{\partial t} + \nabla \cdot (\rho \varepsilon u) = \nabla \cdot \left(\left(\mu + \frac{\mu_t}{\sigma_\varepsilon} \right) \nabla \varepsilon \right) \quad (7)$$

$$+ \rho C_1 E \varepsilon - \rho C_2 \frac{\varepsilon^2}{k + \sqrt{v \varepsilon}}$$

$$G_k = \mu_t \left\{ 2 \left[\left(\frac{\partial u_i}{\partial x_i} \right)^2 + \left(\frac{\partial u_j}{\partial x_j} \right)^2 \right] + \left(\frac{\partial u_i}{\partial x_i} + \frac{\partial u_j}{\partial x_j} \right)^2 \right\} \quad (8)$$

With

$$C_1 = \max\left(0.43, \frac{\eta}{\eta + 5}\right), \eta = \frac{Ek}{\varepsilon}$$

$$E = \left(2E_{ij} \cdot E_{ij} \right)^{1/2}$$

$$E_{ij} = \frac{1}{2} \left(\frac{\partial u_i}{\partial x_j} + \frac{\partial u_j}{\partial x_i} \right)$$

where G_k represents the generation of the turbulence kinetic energy due to the mean velocity gradients, $\sigma_k=1.0$, $\sigma_\varepsilon=1.2$ and $C_2=1.92$. μ_t is the turbulent viscosity, $=C_\mu \rho k^2/\varepsilon$. C_μ is an empirically assigned constant which is set as 0.09 in the simulation.

2.2. Droplet phase

The translational motion of the n th droplet of CO_2 is calculated from the Newtonian equation of motion:

$$\frac{du_{pn}}{dt} = F_D(u - u_{pn}) + \frac{g(\rho_p - \rho)}{\rho_p} + F_n \quad (9)$$

where u_{pn} is the velocity of the n th droplet, $F_D(u - u_{pn})$ is the drag force, ρ_p is the droplet density, and F_n is the sum of the virtual mass force, the force

caused in the rotating coordinate system, Brown force and other forces. F_D can be written as,

$$F_D = -\frac{18\mu}{\rho_p d_p^2} \frac{C_D R_e}{24} \quad (10)$$

Where d_p is the droplet size, and R_e is the relative

Reynold number, $= \frac{\rho d_p |u - u_{pn}|}{\mu}$, and

$$C_D = a_1 + \frac{a_2}{R_e} + \frac{a_3}{R_e^2} \quad (a_1, a_2 \text{ and } a_3 \text{ are constants}).$$

In the near surface layer of earth, the motion of the atmospheric flow is turbulent, and so droplet turbulent dispersion caused by the instantaneous velocity of the gas phase must be considered. Stochastic model is used to describe droplet turbulent dispersion in the paper. The time of the droplet going through gas phase vortex (τ_{cross}) is given by,

$$\tau_{cross} = -\tau \left[1 - \left(\frac{L_e}{\tau |u - u_{pn}|} \right) \right] \quad (11)$$

where L_e is the characteristic length of the gas phase vortex.

The evaporation mass transfer equation for the droplet is

$$\frac{dm_p}{dt} = A_p M k_c \left[\frac{p_{sat}(T_p)}{RT_p} - \alpha_v \frac{p}{RT} \right] \quad (12)$$

where P_{sat} is the saturated vapor pressure corresponding to T_p . T is the temperature of gas phase CO_2 . α_v is the molar volume coefficient. k_c is the coefficient of the mass transfer. Evaporation heat transfer equation of droplet is:

$$m_p c_p \frac{dT}{dt} = h A_p \left[T_\infty - T_p + \frac{dm_p}{dt} h_{fg} \right] \quad (13)$$

where c_p is the specific heat capacity of CO_2 droplet, T_∞ is the temperature of gas phase temperature, and h_{fg} is the latent heat of vaporization of CO_2 droplet.

2.3. Two-way coupling of discrete droplet and continuous gas phase

To achieve more accurate solution of the jet and dispersion of CO_2 from a pressurized transportation pipeline, it is desirable to consider the interactions between discrete droplet and continuous gas phase. When calculating the droplet track, the mass, momentum and energy changes of the droplet are

combined to the source terms of gas phase governing equations to achieve the two-way coupling of discrete droplet and continuous gas phase. Therefore the continuous and discrete phase governing equations were alternately resolved until their convergences.

When the droplet goes through a control volume in the calculation domain, the mass exchange between the droplet and gas phase can be determined by the mass change of the droplet (m_e),

$$m_e = \frac{\Delta m_p}{m_{p,0}} \cdot \dot{m}_{p,0}^* \quad (14)$$

where $\dot{m}_{p,0}^*$ is the initial mass flowrate of the droplet. $m_{p,0}$ is the initial mass of the droplet, and Δm_p is the mass change of the droplet in the control volume.

The momentum exchange (F) equation is given,

$$F = \sum \left(\frac{18\beta\mu c_D R_e}{24\rho_p d_p} (u_{pn} - u_n) + F_n \right) \cdot \dot{m}_{p,0}^* \Delta t \quad (15)$$

where Δt is the time step.

The energy exchange (Q) equation is given,

$$Q = \left[\frac{\overline{m}_p}{m_{p,0}} c_p \Delta T_p + \frac{\Delta m_p}{m_{p,0}} \right] \cdot \dot{m}_{p,0}^* T_{ref} - \left[-h_{fg} + h_{pyrol} + \int_{T_{ref}}^{T_p} c_p dT \right] \quad (16)$$

where \overline{m}_p is the average mass of droplets in the control volume, ΔT_p is the temperature change of droplet, h_{pyrol} is the heat of CO₂ droplet pyrolysis, and T_{ref} is the temperature corresponding to droplet enthalpy.

3. COMPUTATIONAL CONDITIONS

In this paper, a two-dimensional model is established to simulate the jet and dispersion of the leakage source. Fig. 1 shows the two-dimensional model of the jet and dispersion of CO₂ from a pressurized pipeline. The length of the pipeline is 2 m and its internal diameter is 20 mm. The orifice with the diameter of 6 mm is located at the right side of the pipeline. The calculation domain in the flow field is selected as a rectangle with the length of 10 m and width of 3 m. The pressurized pipeline is positioned at the left side of the rectangular region with the height of 1m. The calculation domain is divided with a hexahedron structure grid, and the grids in the local domains around the pipeline, near the leakage orifice and close to the ground surface are refined. Detailed physical and

numerical parameters of CO₂ are summarized in Table 1.

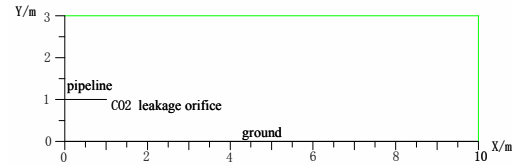


Fig. 1. Two-dimensional model of the jet and dispersion of CO₂

Boundary conditions are specifications of properties on the surfaces of the domains and are required to fully define the flow simulation. Ambient mean wind speed and air temperature profiles are boundary conditions (supposing they are constant over the domain area). The wind speed is zero and temperature is 293 K in this study. The mass flow rate of CO₂ at the leakage orifice also needs to be set in boundary conditions. The initial conditions are 100% mass fraction of CO₂ at the leakage source but

Table 1 Properties of CO₂ droplet

Density (kg/m^3)	1001.6
C_p ($J/kg-K$)	2215.8
Thermal Conductivity ($W/m-K$)	0.1271
Latent Heat (J/kg)	261540
Vaporization Temperature (K)	261.15
Boiling Point (K)	278
Volatile Component Fraction (%)	100
Binary Diffusivity (m^2/s)	$5.728e^{-8}$
Saturation Vapor Pressure (Pa)	Represented by a piecewise linear function
Heat of Pyrolysis (J/kg)	0

0 in other domain. Continuous leakage and instantaneous leakage sources are two classical kinds of leakage sources of CO₂ from high-pressure transportation pipelines. The instantaneous leakage is rare in practical engineering, and thus in this paper, Choked flow, a continuous leakage source, is used to estimate the initial instantaneous mass flow rate of high pressure fluids that have leaked from transportation facilities according to the literature (Perry and Green, 1997). Equation (16) gives the leakage rate of a fluid through an orifice:

$$q = CA \sqrt{k\rho P \left(\frac{2}{n+1} \right)^{(n+1)/(n-1)}} \quad (17)$$

where q is the mass flow rate, C is the discharge coefficient (usually 0.72), A is the discharge orifice cross-sectional area, $=\pi d^2/4$, d is the diameter of the leakage orifice (6 mm), n is the ratio of specific heat of CO₂ (1.29), ρ is the density of CO₂ gas at T and P

(103 kg/m³), P is the absolute upstream pressure (3.95MPa). From Equation (17), the mass flow rate of CO₂ (q) is 0.273 kg/s.

Saturation Vapor Pressure (P_{sat}) is the driving force of CO₂ droplet evaporation. Between the triple point and the critical point of CO₂, its saturation vapor pressure is calculated by

$$\lg P_R = 4.2397 - \left(\frac{4.4229}{T_R}\right) - 5.3795 \lg T_R + 0.1832 \left[P_R / T_R^2 \right] \quad (18)$$

where P_R is the ratio of CO₂ pressure to its critical pressure (P_c), $P_R = P / P_c$, and T_R is the ratio of CO₂ temperature to its critical temperature (T_c).

4. EXPERIMENTAL FACILITY

Figs. 2 and 3 show a schematic diagram and photos of experimental rig of CO₂ leakage. The rig consists of a high pressure CO₂ gas tank, a pressure reducing valve (P1), a transportation pipeline and a throttle valve. The transportation pipeline has the length of 2 m and diameter of 20 mm. The throttle valve is located at the right end of the pipe. The purity of CO₂ in the tank is 99.9% and its pressure is 6 MPa. The throttle valve is a needle valve with the size of 6 mm. Two pressure transmitters (P), two thermocouples (T) and one infrared thermography are used to monitor the jet and dispersion process of CO₂.

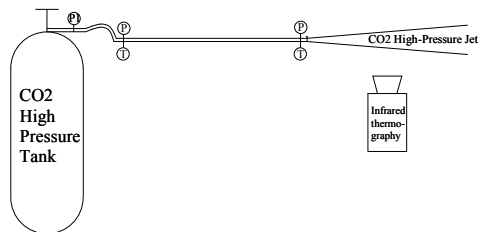


Fig. 2. Schematic diagram of experimental rig of CO₂ leakage



Fig. 3. Photos of experimental rig

The pressure of CO₂ gas from the high-pressure gas tank can be reduced to initial pressures for various experimental cases through use of pressure reducing valve, and then the depressurized CO₂ enters the transportation pipeline. When the needle valve is open, the high pressure CO₂ gas released from the pipeline forms jet flow and disperses into the ambient air. The pressure transmitters and thermocouples are used to monitor the pressure and temperature of CO₂ gas inside pipeline during the leakage process. The infrared thermography is capable of recording the temperature field of CO₂ near the discharge orifice.

5. RESULTS AND DISCUSSIONS

Fig. 4 illustrates the clouds of the mass fraction of CO₂ at $t=8$ s in the calculation domain. As seen in Fig. 4, the jet and dispersion process of CO₂ has the following basic features: (1) Gravitational settling effect. The density of CO₂ gas at room temperature is 1.5 times more than that of the air. The leaked CO₂ from the high pressure pipeline suffers from a pressure drop, which results in a sudden temperature drop of CO₂ due to the Joule-Thomson effect. The leaked CO₂ forms a large area of low temperature CO₂ clouds mixed with CO₂ droplets or dry ice particles on the ground near the leakage orifice due to gravitational settling effect. This is due to the density of CO₂ clouds is dozens or even hundreds of times larger than the air density. Therefore, the high concentrations CO₂ tends to remain close to the surface near the leakage orifice, posing a major health hazard. (2) Turbulent dispersion effect. Near the leakage orifice of the transportation pipeline, CO₂ has obvious gravitational settling effect, and hence CO₂ gas cloud is mainly concentrated in the near surface layer. This is because the Joule-Thompson effect from the pressure change results in low temperature environment and high concentration of CO₂ around the surface. However, away from the leakage orifice, the gravity settling effect gradually weakens due to the increasing environmental temperature, while the effect of atmospheric turbulence is enhanced, and CO₂ gradually disperses to the ambient air and forms dense CO₂ clouds in the air. From Fig. 4, it can be seen that the height of dense CO₂ clouds can reach 2~3 m, not far from the leakage orifice. In this region, dense CO₂ is a serious threat to human life and safety.

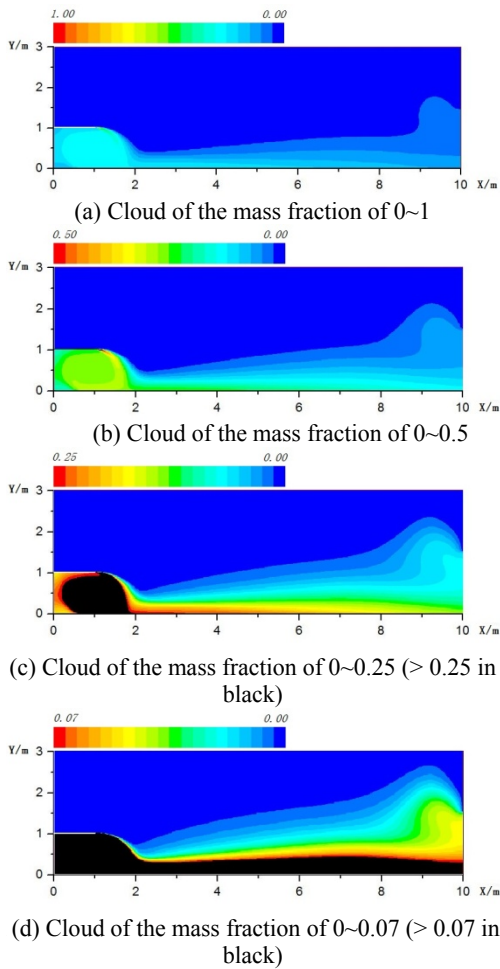


Fig. 4. Clouds of the mass fraction of CO₂ at $t=8$ s in the calculation domain

Fig. 5 shows the cloud of the mass fraction of CO₂ at different times after leakage. From Fig. 5, at initial stage of the leakage, the dispersion of CO₂ cloud is fast in horizontal direction. The heat transfer between CO₂ gas clouds and air is enhanced with time, and so the temperature of the mixed gas rises and its density decreases. CO₂ gradually starts to disperse far from the leakage orifice in the vertical direction. In this stage, the CO₂ cloud is in the passive dispersion state, and continues to disperse to the atmosphere through advection, and the dispersion of CO₂ cloud becomes weak in horizontal direction. This makes gas cloud accumulating on both sides of the cloud, and leads to the occurrence of "arch" phenomenon of the CO₂ cloud.

To clearly illustrate the change of CO₂ concentration with time in the calculation domain, the concentration contour of CO₂ cloud at different times are shown in Fig. 6. In the region far away from the leakage orifice,

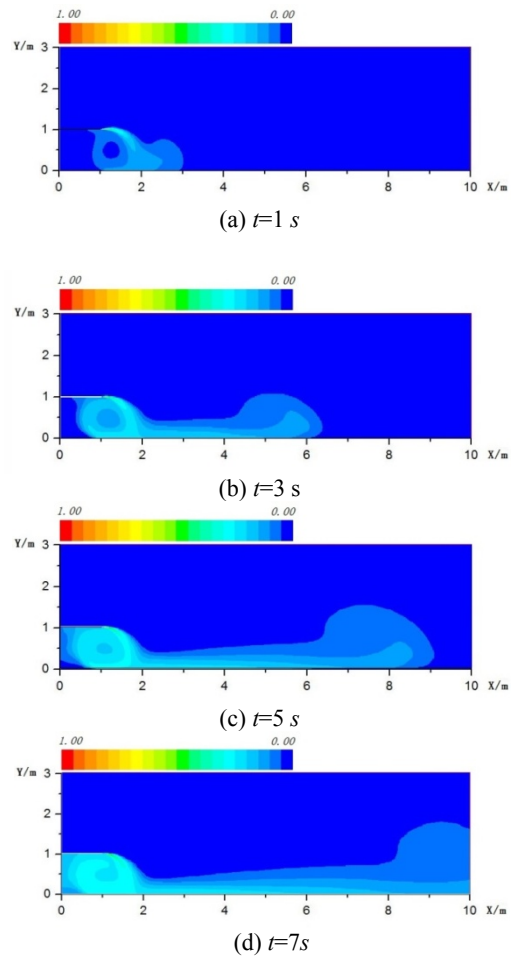
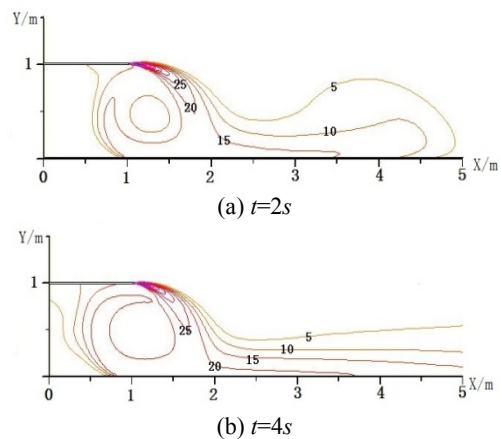


Fig. 5. Cloud of the mass fraction of CO₂ at different times

the concentration of gas cloud varies with time, reaches a maximum and then decreases, and finally tends to constant. Near pipeline leakage orifice, the concentration of gas cloud increases rapidly at the initial stage of leakage, then slows down gradually, and finally tends to be stable.



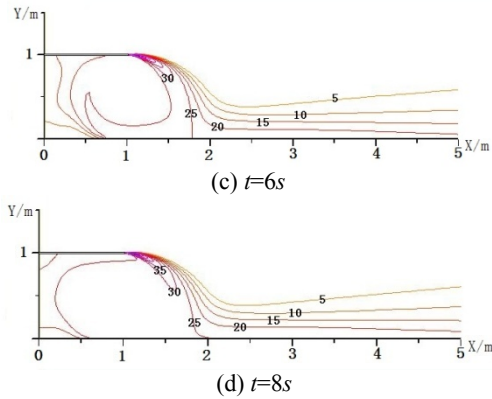


Fig. 6. Concentration contour of CO₂ cloud at different times (mass fraction, %)

Fig. 7 shows the concentration of CO₂ droplet at t=8 s (%). Enlarged drawings of temperature distribution and velocity distribution of CO₂ droplet t=8 s are shown in Fig. 8 and Fig. 9, respectively. From Figs. 7-9, it can be seen that the droplets of CO₂ evaporate quickly due to its intensified heat transfer with ambient air after leakage and exist only in a small area near the leakage orifice.

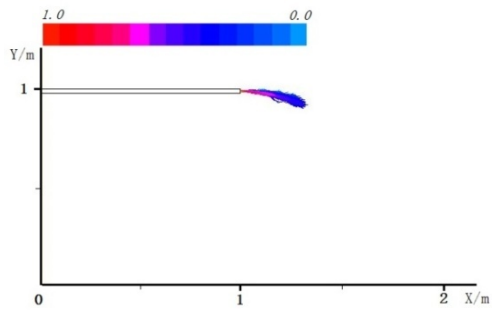


Fig. 7. Mass fraction of CO₂ droplet at t=8 s (%)

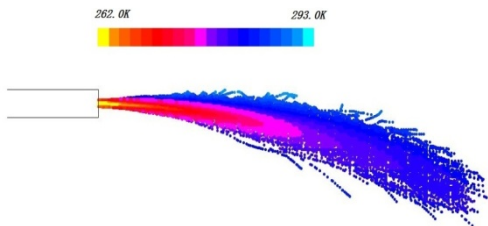


Fig. 8. Temperature distribution of CO₂ droplet t=8 s (K) (Enlarged)

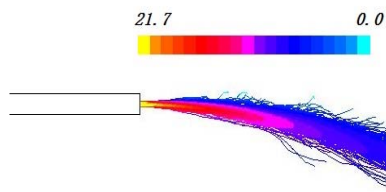
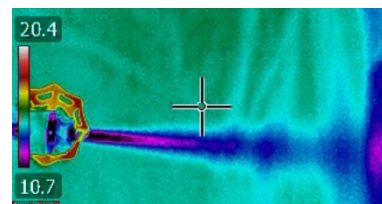


Fig. 9. Velocity distribution of CO₂ droplet t=8 s (m/s) (Enlarged)

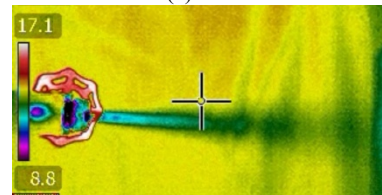
Figs.10-12 shows the variation of the temperature field of CO₂ with time nearby leakage orifice at the initial pressures of 3.95 MPa, 2.96 MPa and 1.94 MPa, respectively. The instantaneous temperature field was recorded by an infrared thermography. As seen in Figs. 10-12, the higher the initial pressure in the pipeline, the more significant the low temperature effect near the leakage orifice. At the initial pressure of 3.95 MPa, the temperature of CO₂ near the leakage orifice decreases rapidly, and reaches the minimum, -11.8 °C, at t=4 s, while at the pressures of 2.96 MPa and 1.94 MPa, the lowest temperatures are 6.3 °C and 8.3 °C, respectively. This can be explained by Joule-Thompson effect. The Joule-Thompson effect describes the relation between the temperature change (ΔT) of a gas and its pressure change (ΔP) when it is forced through a valve.

$$\Delta T = \varphi \cdot \Delta P \quad (19)$$

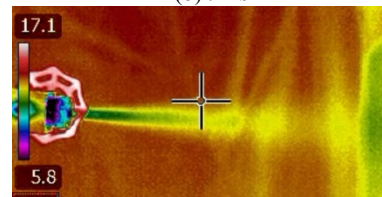
where φ is the J-T coefficient. From Equation (19), it can be seen that there is a linear relationship between the pressure drop and the corresponding gas temperature drop. The higher initial pressure, the larger pressure drop, and thus the more significant cooling phenomenon.



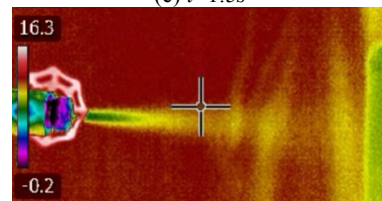
(a) t=0.5s



(b) t=1s



(c) t=1.5s



(d) t=2s

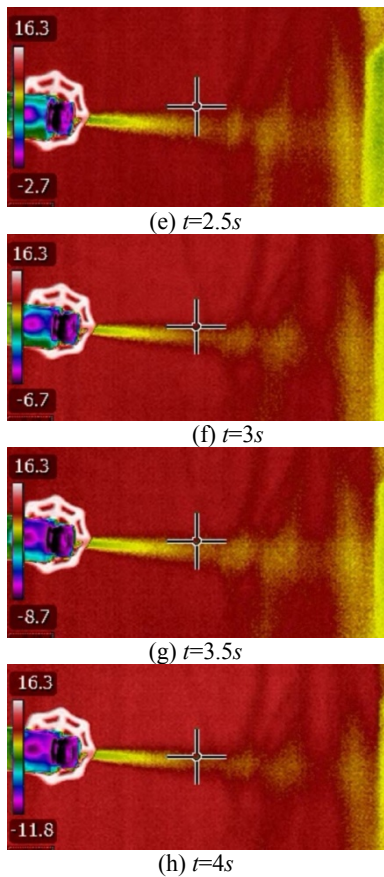


Fig. 10. Variation of the temperature field of CO_2 with time nearby leakage orifice at the initial pressure of 3.95 MPa

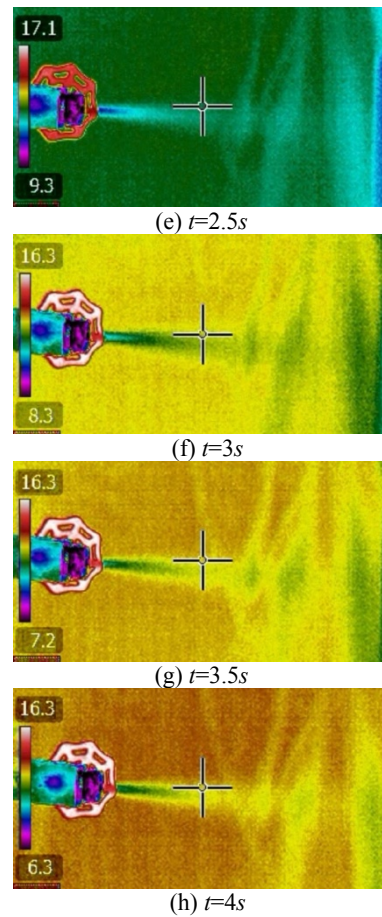
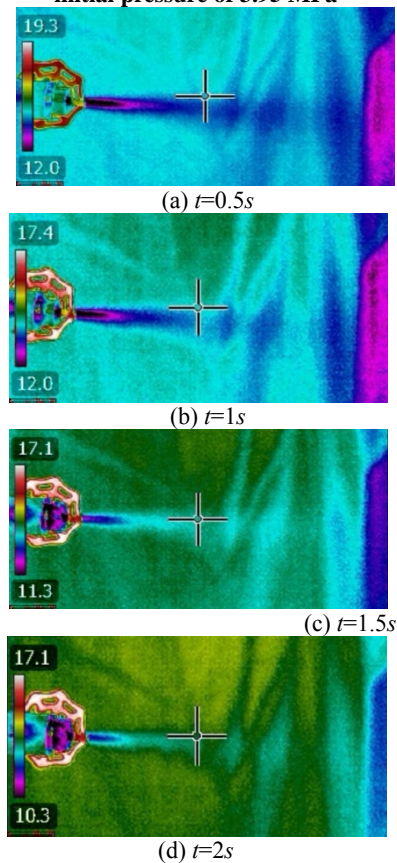
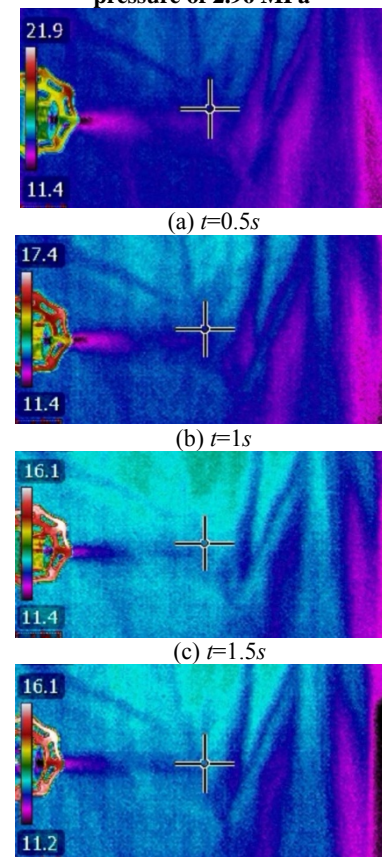


Fig. 11. Variation of temperature field of CO_2 by with time nearby leakage orifice at the initial pressure of 2.96 MPa



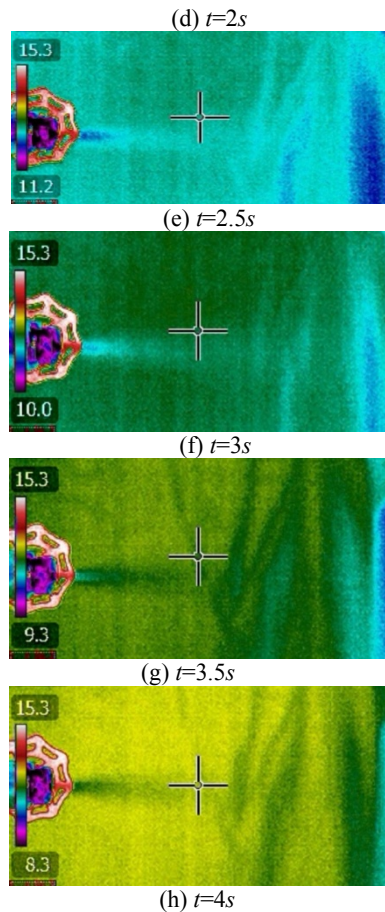
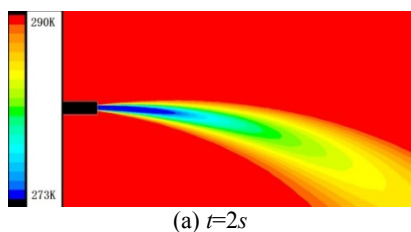
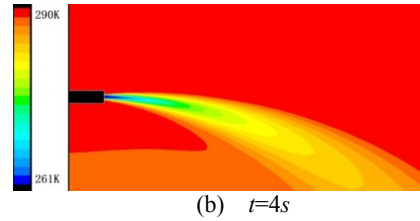


Fig. 12. Variation of temperature field of CO₂ with time nearby leakage orifice at the initial pressure of 1.94 MPa

Fig. 13 shows the calculated temperature field near the leakage orifice at the initial pressures of 3.95 MPa for different times. From Figs.13 and 10, the numerical and experimental results of the temperature field are very similar, validating the reliability of the simulation model. However, there are some differences. The infrared thermography indicates the jet and dispersion of CO₂ have some gravitational settling effect, and yet it is not as significant as the simulation results. This may be caused by the assumption of the uniform and idealized CO₂ droplets and large mass flow rate. In practice the droplets should be different in size. Meanwhile, the delay of the infrared thermography and the consideration of leaked CO₂ as the blackbody also reduce the measurement accuracy, leading to the difference between measurement and numerical results.



(a) $t=2s$



(b) $t=4s$

Fig. 13. Calculated temperature field near the leakage orifice at different times

6. CONCLUSION

In this paper, a two-dimensional model has been developed to study the complex behavior of the jet and dispersion of leaked CO₂ from the pressurized transportation pipeline at continuous leakage flowrate. Euler method has been used to solve the mixture of CO₂ gas and entrained air, the CO₂ droplet evaporation and dispersion was solved by Lagrange method. Considering that CO₂ droplets interact with the surrounding air vortex during leakage, the particle stochastic trajectory model was employed to solve the turbulence and dispersion of CO₂ droplets. A laboratory scale rig for simulating CO₂ pipeline leakage has been built, and the infrared thermography has been used to record the temperature field near the leakage orifice during experiments. Results showed that at the initial stage of the leakage, CO₂ gas has obvious gravitational settling effect. As time goes on, the turbulence dispersion effect is enhanced. The droplets of CO₂ evaporate quickly after leakage and exist only in a small area near the leakage orifice.

ACKNOWLEDGEMENTS

The scientific work was supported by the National Natural Science Foundation of China (No. 51376049), the Natural Science Foundation of Jiangsu Province for Distinguished Young Scholars (No. BK20150023) and Marie Curie Actions – International Research Staff Exchange Scheme, Seventh Framework Program, European Commission (No. FP7-PEOPLE-2013-IRSES /612230). The authors also would like to acknowledge the Royal Academy of Engineering (UK) that provided Newton International Fellowship Alumni Follow-on Funding in collaboration with the University of Kent, UK.

REFERENCES

- Cortis, A. (2009). Oldenburg Short-range atmospheric dispersion of carbon dioxide. *Boundary-layer Meteorology* 133(1), 17-34.
- Eldevik, F., B. Graver and L. E. Torbergsen (2009). Development of a guideline for safe, reliable and cost efficient transmission of CO₂ in pipelines. *Energy Procedia* 1(1), 1579-1585.
- Molag, M. and C. Dam (2011). Modelling of accidental releases from a high pressure CO₂ pipelines. *Energy Procedia* 4(1), 2301-2307.

- Mazzoldi, A., T. Hill and J. Colls (2008a). CO₂ transportation for carbon capture and storage: Sublimation of carbon dioxide from a dry ice bank. *International Journal of Greenhouse Gas Control* 2(2), 210-218.
- Mazzoldi, A., T. Hill and J. J. Colls (2008b). CFD and Gaussian atmospheric dispersion models: A comparison for leak from carbon dioxide transportation and storage facilities. *Atmospheric Environment* 42(34), 8046-8054.
- Mazzoldi, A., T. Hill and J. J. Colls (2009). A Consideration of the jet-mixing effect when modelling CO₂ emissions from high pressure CO₂ transportation facilities. *Energy Procedia* 1(1), 1571-1578.
- Mazzoldi, A., T. Hill and J. J. Colls (2011). Assessing the risk for CO₂ transportation within CCS projects, CFD modeling. *International Journal of Greenhouse Gas Control* 5(4), 816-825.
- Perry, R. H. and D. W. Green (1997). *Perry's Chemical Engineers' Handbook*. New York, America: McGraw-Hill.
- Svensson, R., M. Odenberger and F. Johnsson (2004). Transportation systems for CO₂ application to carbon capture and storage. *Energy Conversion and Management* 45(15), 2343-2353.
- Vagesh, D. and A. S. GexCon (2013a). FLACS model developments including the source, wind and terrain models. Technical Report of FP7 Project CO₂ PipeHaz.
- Vagesh, D. and A. S. GexCon (2013b). On the validation studies of two-phase models in FLACS and CFX. Technical Report of FP7 Project CO₂ PipeHaz.
- Witlox, H. W. M., M. Harper and A. Oke (2009). Modelling of discharge and atmospheric dispersion for carbon dioxide releases. *Journal of Loss Prevention in the Process Industries* 22(6), 795-802.